Nanoscale

PAPER

View Article Online
View Journal | View Issue

Cite this: *Nanoscale*, 2015, **7**, 7252

High-performance flexible photodetectors based on GaTe nanosheets

Zhenxing Wang,† Muhammad Safdar,† Misbah Mirza, Kai Xu, Qisheng Wang, Yun Huang, Fengmei Wang, Xueying Zhan and Jun He*

2D layered GaTe materials have attracted a great deal of attention for optoelectronic applications due to their direct band structure, whether in bulk or as a single layer. In this paper, for the first time, we have synthesized high quality, single crystalline GaTe nanosheets by employing a facile CVD method. The size of the GaTe nanosheets reached several tens of micrometers, and some of them even exceeded 100 μm. In particular, planar GaTe nanosheets were achieved on a mica substrate following a van der Waals epitaxial growth mechanism. Further, through a systematic comparison of the performances under various conditions, we found that adsorbates on the GaTe surface under ambient conditions strongly deteriorated the GaTe photodetector device performance. After removing the adsorbates in a ~7 × 10^{-5} torr vacuum, a flexible, fast response GaTe photodetector with a high photoresponse, high mechanical stability and an excellent linear input–output relationship was obtained. The results presented in this study suggest that the GaTe nanosheets grown by a CVD method are promising candidates for optoelectronic applications in the future.

Received 11th December 2014,
Accepted 18th March 2015

DOI: 10.1039/c4nr07313d

www.rsc.org/nanoscale

Introduction

Two-dimensional semiconducting metal chalcogenides (2D-SMCs) have attracted intensive interest over the past decade due to their unique electronic and optoelectronic attributes.[1–6] Researchers have been trying to find materials compatible with silicon in the field of electronics and optoelectronics. On the one hand, 2D-SMCs exhibit similar properties to traditional silicon semiconductors, for example suitable energy band gaps for solar energy conversion (around 1–2 eV). On the other hand, their special characteristics, such as layered crystal structures and direct energy band alignments, make them more attractive in optoelectronic devices. Although the conventional III–V group materials also have direct energy band structures and very high carrier mobility performances, 2D-SMCs are still more competitive due to their advantages of flexibility, relatively high earth abundance, high degree of electrostatic control and relative ease of material growth and device fabrication. Moreover, various novel physics in 2D-SMC materials, such as thickness-dependent band gap transitions,[7] valley-related spintronics,[8–10] ambipolar behavior[11–13] and tunable excitonic effects,[14] make them scientifically important in fundamental research for practical applications. So far, a large number of 2D-SMC materials, including transition metal dichalcogenides (TMDCs) MX_2 (M = Mo, W, Re; X = S, Se, Te),[4,15–19] III–VI group chalcogenides MX (M = In, Ga; X = S, Se, Te),[20–24] and IV–VI group chalcogenides MX (M = Ge, Sn; X = S, Se),[25–28] have been investigated for applications such as field effect transistors, phototransistors, flexible and transparent photodetectors, and photovoltaic cells.

Gallium telluride (GaTe) is an important III–VI layered semiconducting material, which has a monoclinic crystal structure in the space group C_{2h}^3 and consists of vast individual layers bonded together by weak van der Waals' interactions.[29] Two kinds of different Ga–Ga bonds exist: one-third are parallel and two-thirds are perpendicular to the layer, as shown in Fig. 1a. GaTe has a direct band gap of around 1.7 eV in both the single layer and bulk forms at room temperature.[29–31] This implies that GaTe may have excellent optoelectronic properties even in its multilayer state. It is better than most TMDC materials, which have direct band structures in only the single-layer form. Because of the direct band gap, Liu *et al.* demonstrated a photosensitive device based on GaTe nanoflakes with a remarkable photoresponsivity of 10^4 A W^{-1}, which is much better than that of graphene and MoS_2.[30] Hu *et al.* reported a GaTe nanosheet photodetector exhibiting a very high detectivity of ~10^{12} Jones, which even exceeds that of the currently-exploited InGaAs photodetectors (10^{11}–10^{12}).[32] Recently, through both electrical measurements at various temperatures and theoretical simulations, we found that Ga vacancies play a critical role in

National Center for Nanoscience and Technology, Beijing 100190, P. R. China. E-mail: hej@nanoctr.cn
† These authors contributed equally to this work.

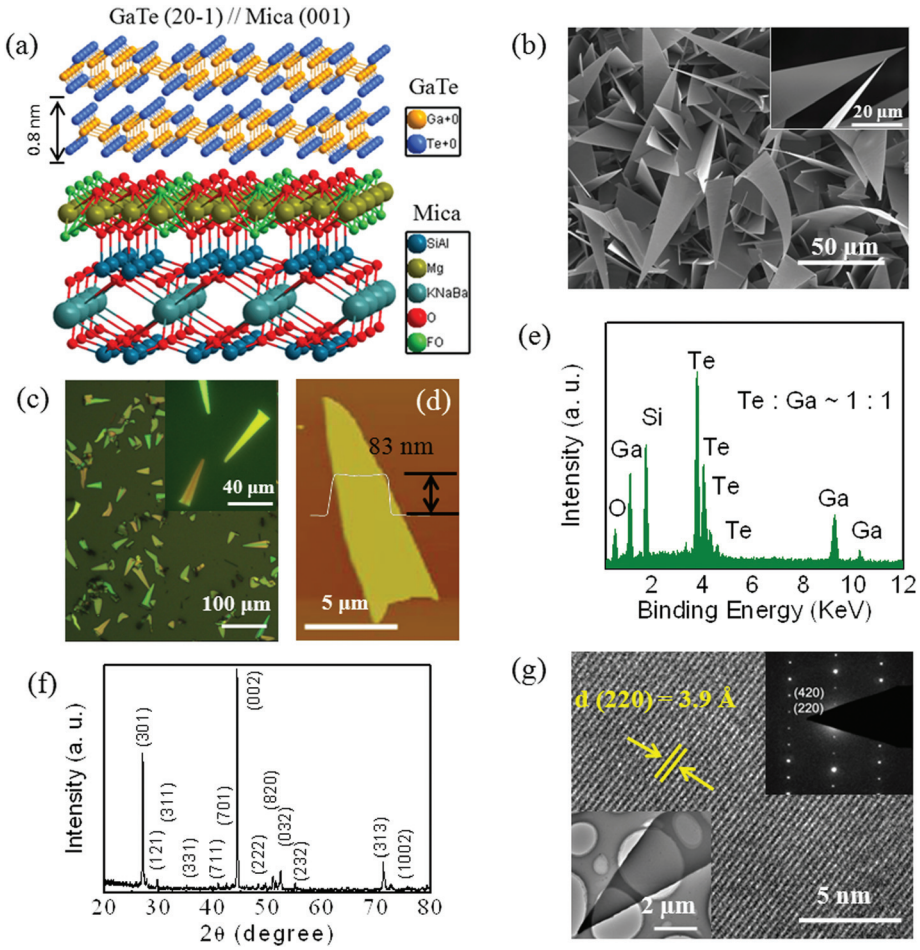

Fig. 1 Characterization of the GaTe nanosheets. (a) Scheme of the crystal structures: GaTe on mica. The GaTe (20-1) plane is parallel to the mica (001) plane. (b) A typical SEM image of the as-grown GaTe nanosheets on the SiO_2/Si substrate by the CVD method. Inset: enlarged SEM image. (c) An optical image of the as-grown GaTe nanosheets on a mica substrate. Inset: magnified optical image. (d) An AFM image of a triangular GaTe nanosheet. (e) X-ray EDS of the GaTe nanosheets. (f) X-ray diffraction pattern of the as grown GaTe nanosheets. (g) An HRTEM image of a typical GaTe nanosheet. Insets: SAED pattern (top) and a low magnification TEM image (bottom).

the performance of GaTe field-effect transistors (FETs). After suppressing the Ga vacancy defects, a high performance GaTe phototransistor was achieved.[20] The above results strongly indicate that 2D GaTe nanosheets are a promising candidate for optoelectronic applications. However, we notice that all work published before is based on mechanically exfoliated GaTe nanosheets. It is well known that the mechanical exfoliation method can easily fabricate few-layer and even monolayer 2D materials with high purity for scientific fundamental research. However, for practical applications, a more effective, controllable, uniform material preparation method is highly desired. Chemical vapor deposition is considered to be the most promising route by precisely adjusting the growth parameter and precursor stoichiometry.

In this report, for the first time, we have synthesized single crystalline GaTe nanosheets by a chemical vapour deposition (CVD) method. Through choosing a suitable growth mode, the grown GaTe nanosheet orientation can be effectively controlled. In particular, when employing mica as the growth substrate, GaTe nanosheets with planar alignments can be obtained, which follow a van der Waals epitaxial growth mechanism by taking advantage of the chemically inert surface of mica. The GaTe sizes of both the vertical and lateral arrays approach several tens of micrometers, and even exceed 100 micrometers. Further, the GaTe nanosheet photodetectors were systematically investigated on both rigid substrates (SiO_2/Si) and flexible substrates (polyethylene terephthalate, PET). By comparing the photoresponse properties under different conditions, such as ambient, vacuum, 375 nm laser and 473 nm laser, we found that the surface adsorbates under ambient conditions strongly affect the performance of the device. By pumping the vacuum to $\sim 7 \times 10^{-5}$ torr, a high performance flexible photodetector was achieved. The device exhibits a relatively fast response and recovery time (~50 ms), a linear input–output relationship, and a very high photoresponse stability and mechanical stability. These results show that GaTe nanosheets grown by the CVD method are promising materials for high-performance photodetectors on both rigid and flexible substrates.

Experimental section

Growth of 2D GaTe nanosheets by the CVD method

GaTe nanosheets were synthesized in a horizontal tube furnace with a 1 inch diameter *via* a chemical vapor deposition method, with a similar setup to our previous In_2Te_3 and WSe_2 growth methods.[16,33] In brief, GaTe powder (99.99%, Alfa Aesar) used as the source was placed at the center of the tube. A silicon wafer with a 300 nm thick oxidation layer or cleaved fresh mica was used as the growth substrate and was put downstream ~5 cm away from the source. Prior to growth, the tube was pumped to a vacuum below 1 Pa and flushed with Ar gas three times to remove the oxygen residue. Then, the furnace temperature was increased to 750 °C at a rate of 30 °C min^{-1} under 50 sccm Ar gas. After 20 min, the furnace was cooled down to room temperature under Ar gas flow.

Characterization of the as-grown GaTe nanosheets

The resulting samples were characterized by AFM (Veeco Multimode), FESEM (Hitachi S-4800) equipped with an X-ray energy dispersive spectrometer (EDS), optical microscopy (OM, Olympus BX51M), HRTEM (FEI20) and XRD (D/Max-TTRIII diffractometer) using Cu K_α radiation (λ = 1.5418 Å).

Device fabrication and measurements

The nanosheets were released into ethanol by sonication of the growth substrate and then further transferred onto a silicon wafer with a 300 nm thick oxidation layer for the rigid devices and PET for the flexible devices. The electrical contacts were obtained by evaporating 8 nm Cr and 150 nm Au, utilizing a copper grid as a shadow mask with a typical gap of 15 μm. The electrical transport measurements were performed on a probe station (Lakeshore, TTP4) equipped with a vacuum pump and a semiconductor characterization system (Keithley 4200). The photoresponse properties were examined by employing a 473 nm laser (RGBLase LLC) and 375 nm laser (RGBLase LLC).

Results and discussion

Fig. 1b shows a typical top-view field emission scanning electron microscopy (FESEM) image of the as-grown GaTe nanosheets on a SiO_2/Si substrate by the CVD method. It explicitly indicates that the product has a high density, triangular shape and smooth surface. Moreover, to our surprise, the size of most of the GaTe nanosheets was several tens of micrometers, and some of them even exceeded 100 μm, which is much larger than those of MoS_2, WSe_2 and GaSe grown by the CVD method.[16,23,34] Furthermore, we note that the growth of the GaTe arrays on the SiO_2/Si substrates is very different from other layered 2D-SMC materials, for example MoS_2 and WS_2. The latter laterally grows along the substrate surface, however the former vertically aligns to the substrate. This result may be due to the presence of dangling bonds at the SiO_2/Si surface, which increases the energy barrier for migration of the GaTe adatom along the substrate surface. Recently, fluorophlogopite has been widely used for aligned orientation of the van der Waals epitaxial growth of 2D layered chalcogenide nanosheets because mica has a chemically inert surface without dangling bonds.[35,36] To obtain the planar GaTe nanosheets, a layered mica sheet was utilized as the growth substrate. As expected, Fig. 1c evidently reveals that the GaTe nanosheets lie on the mica substrate with a large lateral dimension, uniform thickness and smooth surface. A tentative crystal structure model for the van der Waals epitaxial growth is shown in Fig. 1a. The mica substrate used here is critical for the formation of planar GaTe nanosheets. On the one hand, the chemically inert mica surface enables the lateral epitaxial growth of GaTe nanosheets without strict lattice matching. On the other hand, weak van der Waals interactions between the mica substrate and GaTe adatoms facilitate the lateral migration of the GaTe adatoms, and thus promote the lateral growth of the GaTe nanosheets. In contrast to the planar arrays on mica substrates, the GaTe nanosheets grow on Si/SiO_2 substrates in randomly aligned arrays under exactly the same growth conditions. This definitely confirms the van der Waals epitaxial effect of GaTe nanosheets on mica substrates. The atomic force microscopy (AFM) image further shows that the thickness of a typical GaTe sheet is about 80 nm and it has a smooth surface, as shown in Fig. 1d. The X-ray energy dispersive spectrum (EDS) acquired from one single GaTe nanosheet (Fig. 1e) exhibits strong Ga and Te signals and confirms that the atomic ratio of Ga : Te is very close to the stoichiometric 1 : 1 ratio of GaTe.

To investigate the crystallinity, X-ray diffraction (XRD) and high resolution transmission electron microscopy (HRTEM) were performed on the GaTe nanosheets. The XRD pattern in Fig. 1f clearly depicts the main peaks at 2θ = 26.7°, 27.8°, 44.3°, and 52.3°, which correspond to the (301), (121), (002), and (032) planes, respectively. The pattern is consistent with JCPDF 65-0028, which confirms the as-grown GaTe sheets belong to the monoclinic crystal structure. Fig. 1g gives a typical HRTEM image and a lattice fringe is observed with an interplane spacing of 3.9 Å, corresponding to the (220) plane. The selected area electron diffraction (SAED) pattern (inset in Fig. 1g) indicates that the GaTe nanosheet is formed from single crystals. All the above characterization results suggest that our CVD method is a promising route to produce GaTe nanosheets with a high density, uniform thickness and high crystal quality. By selecting a suitable substrate and precisely controlling the temperature, gas flow rate and substrate position during the growth process, GaTe nanosheets with high quality and yield were achieved.

To study the transport properties of the as-synthesized GaTe nanosheets, a single nanosheet-based FET was fabricated by evaporating 8 nm/150 nm Cr/Au metal contacts using a copper grid as a shadow mask, as shown in the inset of Fig. 2a. The inset of Fig. 2b shows an optical image of a representative GaTe nanosheet device on a Si substrate with a 300 nm thermal oxidation layer and a device channel length of 20 μm and a width of 37 μm. The transfer curve was measured

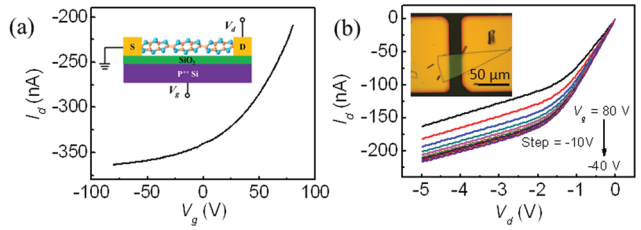

Fig. 2 Transport measurements of the GaTe nanosheet device. (a) Transfer curve (source–drain voltage, V_d = −5 V) and (b) output characteristics of a back-gated GaTe transistor measured under ambient conditions. Insets in panels (a) and (b): scheme and an optical image of the GaTe device.

under the back-gated voltage, scanning from 80 V to −80 V under ambient conditions, as shown in Fig. 2a. From the transfer curve, it can be seen that the drain current increases with the gate voltage scanning from positive to negative, indicating p-type semiconductor behavior. The output characteristics in Fig. 2b further confirm the p-type behavior of the GaTe device. The device exhibits a clear current saturation at high V_d, which is probably due to the pinch-off phenomenon, similar to traditional metal oxide semiconductor FETs. It is worth noting that the GaTe channel cannot be completely switched off by the gate voltages. The relatively poor transport behavior is most likely due to the generated defects or vacancies during the growth and the relatively large channel thickness.

As mentioned in the introduction, GaTe shows great potential for highly sensitive photodetectors and phototransistors since it has a direct band structure.[20,30,32] To check the photoresponse properties of our grown GaTe nanosheets, both rigid and flexible devices were fabricated. The transport and photoresponse properties of GaTe are strongly affected by the surface adsorbates. Fig. 3a shows the *I–V* curves of the GaTe device on a rigid substrate measured under ambient and vacuum conditions. It was found that the *I–V* curve measured under ambient conditions exhibits a little nonlinearity, which should be attributed to the Schottky barrier contact arising from the slight mismatch of the work functions between the Cr/Au electrodes and the GaTe nanosheet. After the device was pumped to around 10^{-5} torr and held for 4 h under vacuum, the *I–V* curve shows excellent linearity, corresponding to the Ohmic contacts. The improvement in the electrode contacts can be attributed to the lowering of the Schottky barrier between the work function of Cr and the valence band maxima of GaTe by removing the GaTe surface adsorbates.[37] A similar improvement in the metal-semiconductor contact was observed in Fig. 3b by utilizing a 375 nm laser to irradiate GaTe under ambient conditions. It should be noted that the 473 nm laser cannot promote the electrical contact. The difference in the photoresponse between visible light and UV light was also found in our previous work on In_2Te_3.[33] To further uncover the intrinsic mechanism, we investigated the time-resolved photoresponse of the GaTe device with the 375 nm and 473 nm lasers on and off. From Fig. 3b and c, three

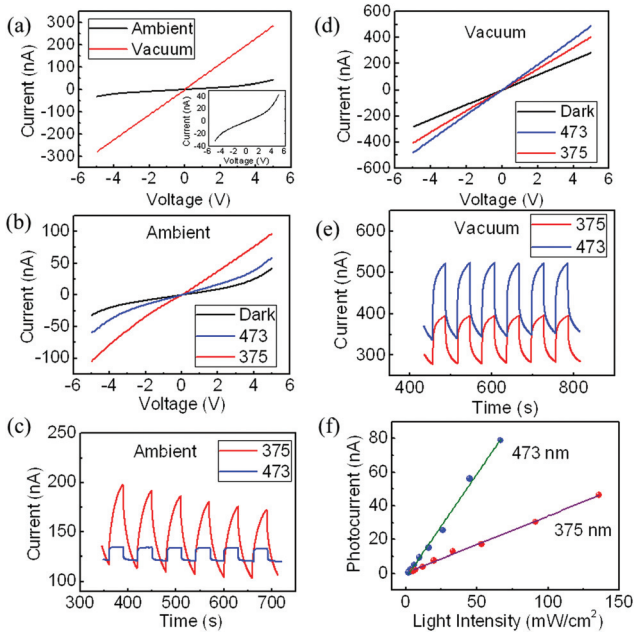

Fig. 3 Transport and photoresponse measurements. (a) *I–V* curves of the GaTe device under ambient and vacuum (7×10^{-5} torr) conditions measured by a two-terminal method. Inset: enlarged *I–V* curve under ambient conditions. The *I–V* curves of the same device under (b) ambient and (d) vacuum conditions in the dark and illumination from the 473 and 375 nm lasers. Time resolved photoresponse of the GaTe device recorded by alternatively switching on and off the laser under (c) ambient and (e) vacuum conditions. Note: the above power intensity is 163.9 and 80.5 mW cm^{-2} for the 375 and 473 nm lasers, respectively. (f) Light intensity dependence of the photocurrent under illumination from the 473 and 375 nm lasers. The bias is 5 V for (c, e and f).

typical features should be noted. The first is that for both the 375 nm and 473 nm lasers, the baseline (dark-current) and photocurrent shift to a higher current level during long time illumination, compared to the dark current shown in Fig. 3b. The second is that the 375 nm laser can improve the electrical contact, however the 473 nm laser cannot. The last is that the response and recovery speed with the 375 nm laser exhibit slower kinetics than with the 473 nm laser. The first feature probably originates from the adsorption and desorption process of surface gas molecules by a laser heating effect.[38] The second and third features are mostly related to an O_2 doping GaTe process by the 375 nm laser, like a UV-ozone doping process.[39] The slow doping course generates corresponding slow photoresponse kinetics. As a distinctive contrast, the device under vacuum exhibits a better performance than under ambient conditions, as shown in Fig. 3d and e. All of the *I–V* curves show excellent linearity. Eliminating the influences from the surface adsorbates, the photoresponse properties display a high stability and similar rise and reset time for both the 375 nm and 473 nm lasers. Importantly, the photocurrent has a linear relationship with the incident light intensity, as shown in Fig. 3f, which indicates that the GaTe photodetector is a typical photon-dependent resistor.[40]

Research on flexible devices has been one of the most attractive topics for promising next-generation candidates for electronics and optoelectronics, such as portable devices, aerospace science and civil engineering.[21,41–44] To measure the performance of the GaTe nanosheet photodetector on a flexible substrate, the grown GaTe nanosheets were transferred onto a PET substrate and subsequently Cr/Au metal contacts were patterned using a copper grid shadow mask. Fig. 4a shows a typical optical image of a flexible GaTe device. The device channel was around 14 μm in length and 12 μm in width. The laser with 473 nm wavelength and 80.5 mW cm^{-2} power intensity was employed in the flexible photoresponse measurements. To eliminate the influence from the surface adsorbates, all measurements were performed under vacuum. Fig. 4b depicts the *I–V* curves in the dark and under laser illumination before and after bending the device. Both the *I–V* curves after bending 100 and 200 times show excellent agreement with the original data, whether under dark conditions or under the laser illumination. This indicates the flexible GaTe photodetector has a high stability. To further confirm the high stability of the mechanical bend and photoresponse, time evolutions of the photoresponse before bending and after bending 100 times and 200 times were measured at a fixed bias voltage of 5 V, as shown in Fig. 4c. With the laser irradiation on and off, the current shows an "off-state" current of ~0.38 nA and an "on-state" current of ~4.27 nA, giving an on/off ratio of 11. This indicates that the GaTe nanosheet photodetector is highly responsive. More importantly, for every separated *I–t* curve, the six "on"–"off" cycles retain a very similar dark current, photocurrent and noise level, which manifest the high reversibility and photoresponse stability of the device. Additionally, the "on-state" current before bending and after bending shows very little difference and is estimated to be below 4%. These results further prove the excellent mechanical stability of the flexible device.

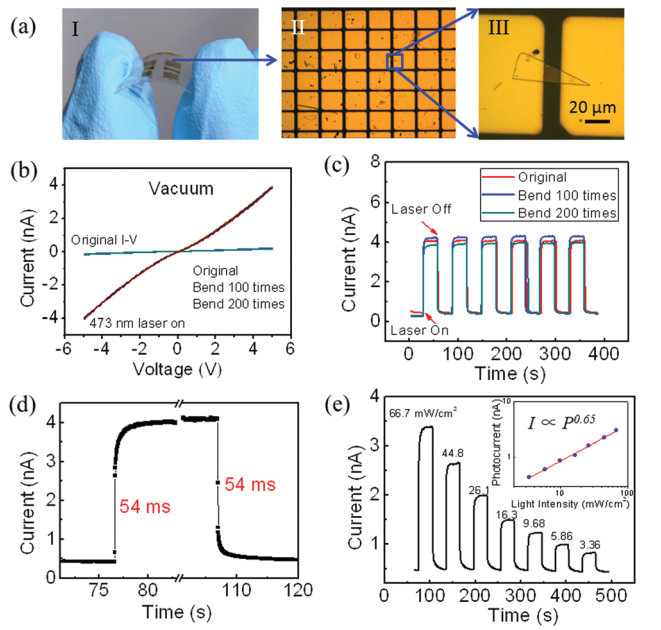

Fig. 4 Flexible GaTe nanosheet photodetector. (a) Optical images of the GaTe nanosheet device on a PET substrate. (b) *I–V* curves of the flexible device under vacuum (7×10^{-5} torr) in the dark and illumination by a 473 nm laser with 80.5 mW cm^{-2} power intensity after bending 100 and 200 times. (c) Time-dependent photoresponse of the same device with the laser on and off after bending different times at a bias of 5 V. (d) One single photoresponse cycle. (e) Photocurrent under laser conditions with different powers at the same bias of 5 V. Inset: photocurrent as a function of light intensity.

The response and reset time, photoresponsivity (R_λ), external quantum efficiency (EQE) and the relationship between the input and output are also critical parameters for a flexible photodetector as well as the stability. Fig. 4d depicts a single photoresponse cycle containing the rise and reset process. Once the laser was switched on or off, the photocurrent dramatically increased or decreased more than 67% in the initial 54 ms. After the initial 54 ms, the photocurrent changed to a little slower kinetics, which may be attributed to the influences of the vacancies, trap states and other defects.[20] The rise and decay time are closely comparable to the data reported for other layered material-based photodetectors.[22,45] Considering the GaTe device is a typical photoconductor and has a thick and long conducting channel, the response and reset time are relatively fast. The relationship between the incident light intensity and photocurrent was also investigated. Fig. 4e shows that the photocurrent reduces in a step-like manner as the light intensity decreases. The photocurrent can be expressed by a power law equation, $I_{ph} \propto P^{\alpha}$, where I_{ph} is the photocurrent, P is the light intensity, and α is the index of a power law. As shown in the inset of Fig. 4e, by fitting the experimental data, the α value was calculated to be 0.65. The deviation from the ideal index of $\alpha = 1$ implies the loss of light energy during the conversion from external light energy to current, which is related to complex processes in photon absorption, electron–hole separation and carrier transfer.[46] Additionally, to obtain the ideal α value, the crystal quality should be improved, thus reducing the trap states and vacancies. The photoresponsivity $R_\lambda = I_{ph}/(PS)$ and the EQE $= hcR_\lambda/(e\lambda)$, where I_{ph} is the photogenerated current, P is the incident light intensity, S is the effective illuminated area, h is Plank's constant, c is the light velocity, e is the electronic charge, and λ is the incident light wavelength. Based on the device configuration (Fig. 4a-III) and measured data, R_λ and EQE were calculated to be 0.03 A W^{-1} and 8% at a light intensity of 80.5 mW cm^{-2}.

Conclusions

In conclusion, for the first time, single crystalline GaTe nanosheets were efficiently synthesized by a simple CVD method. Depending on the growth substrates, the GaTe orientation can be controlled. In particular, by introducing a van der Waals epitaxial growth mechanism on a mica substrate, planar GaTe nanosheets were achieved. The lateral size of the nanosheets can be above 100 μm. Further, both rigid and

flexible GaTe photodetectors were fabricated and the corresponding photoresponse properties were carefully studied under various conditions. We found that adsorbates on the GaTe surface under ambient conditions strongly deteriorated the device performance. By removing the adsorbates in a $\sim 7 \times 10^{-5}$ torr vacuum, a flexible GaTe photodetector with a fast response and reset time, a high stability and an excellent linear input–output relationship was obtained. These results make GaTe nanosheets a strong candidate for constructing novel rigid and flexible optoelectronic devices.

Acknowledgements

This work was supported by the 973 Program of the Ministry of Science and Technology of China (no. 2012CB934103), the 100-Talents Program of the Chinese Academy of Sciences (no. Y1172911ZX), the National Natural Science Foundation of China (Nos. 21373065 and 61474033) and Beijing Natural Science Foundation (no. 2144059).

Notes and references

1 M. Chhowalla, H. S. Shin, G. Eda, L. J. Li, K. P. Loh and H. Zhang, *Nat. Chem.*, 2013, **5**, 263–275.
2 O. Lopez-Sanchez, D. Lembke, M. Kayci, A. Radenovic and A. Kis, *Nat. Nanotechnol.*, 2013, **8**, 497–501.
3 R. Mas-Balleste, C. Gomez-Navarro, J. Gomez-Herrero and F. Zamora, *Nanoscale*, 2011, **3**, 20–30.
4 B. Radisavljevic, A. Radenovic, J. Brivio, V. Giacometti and A. Kis, *Nat. Nanotechnol.*, 2011, **6**, 147–150.
5 C. N. R. Rao, H. Matte and U. Maitra, *Angew. Chem., Int. Ed.*, 2013, **52**, 13162–13185.
6 Q. H. Wang, K. Kalantar-Zadeh, A. Kis, J. N. Coleman and M. S. Strano, *Nat. Nanotechnol.*, 2012, **7**, 699–712.
7 K. F. Mak, C. Lee, J. Hone, J. Shan and T. F. Heinz, *Phys. Rev. Lett.*, 2010, **105**, 136805.
8 S. F. Wu, C. M. Huang, G. Aivazian, J. S. Ross, D. H. Cobden and X. D. Xu, *ACS Nano*, 2013, **7**, 2768–2772.
9 T. Cao, G. Wang, W. P. Han, H. Q. Ye, C. R. Zhu, J. R. Shi, Q. Niu, P. H. Tan, E. Wang, B. L. Liu and J. Feng, *Nat. Commun.*, 2012, **3**, 887.
10 K. F. Mak, K. L. He, J. Shan and T. F. Heinz, *Nat. Nanotechnol.*, 2012, **7**, 494–498.
11 W. Liu, J. H. Kang, D. Sarkar, Y. Khatami, D. Jena and K. Banerjee, *Nano Lett.*, 2013, **13**, 1983–1990.
12 D. Braga, I. G. Lezama, H. Berger and A. F. Morpurgo, *Nano Lett.*, 2012, **12**, 5218–5223.
13 Y. J. Zhang, J. T. Ye, Y. Matsuhashi and Y. Iwasa, *Nano Lett.*, 2012, **12**, 1136–1140.
14 J. S. Ross, S. F. Wu, H. Y. Yu, N. J. Ghimire, A. M. Jones, G. Aivazian, J. Q. Yan, D. G. Mandrus, D. Xiao, W. Yao and X. D. Xu, *Nat. Commun.*, 2013, **4**, 1474.
15 S. Tongay, H. Sahin, C. Ko, A. Luce, W. Fan, K. Liu, J. Zhou, Y. S. Huang, C. H. Ho, J. Y. Yan, D. F. Ogletree, S. Aloni, J. Ji, S. S. Li, J. B. Li, F. M. Peeters and J. Q. Wu, *Nat. Commun.*, 2014, **5**, 3252.
16 K. Xu, Z. X. Wang, X. L. Du, M. Safdar, C. Jiang and J. He, *Nanotechnology*, 2013, **24**, 465705.
17 M. Yamamoto, S. T. Wang, M. Y. Ni, Y. F. Lin, S. L. Li, S. Aikawa, W. B. Jian, K. Ueno, K. Wakabayashi and K. Tsukagoshi, *ACS Nano*, 2014, **8**, 3895–3903.
18 X. M. Zou, J. L. Wang, C. H. Chiu, Y. Wu, X. H. Xiao, C. Z. Jiang, W. W. Wu, L. Q. Mai, T. S. Chen, J. C. Li, J. C. Ho and L. Liao, *Adv. Mater.*, 2014, **26**, 6255–6261.
19 H. Qiu, T. Xu, Z. L. Wang, W. Ren, H. Y. Nan, Z. H. Ni, Q. Chen, S. J. Yuan, F. Miao, F. Q. Song, G. Long, Y. Shi, L. T. Sun, J. L. Wang and X. R. Wang, *Nat. Commun.*, 2013, **4**, 2642.
20 Z. X. Wang, K. Xu, Y. C. Li, X. Y. Zhan, M. Safdar, Q. S. Wang, F. M. Wang and J. He, *ACS Nano*, 2014, **8**, 4859–4865.
21 P. A. Hu, L. F. Wang, M. Yoon, J. Zhang, W. Feng, X. N. Wang, Z. Z. Wen, J. C. Idrobo, Y. Miyamoto, D. B. Geohegan and K. Xiao, *Nano Lett.*, 2013, **13**, 1649–1654.
22 P. A. Hu, Z. Z. Wen, L. F. Wang, P. H. Tan and K. Xiao, *ACS Nano*, 2012, **6**, 5988–5994.
23 Y. B. Zhou, Y. F. Nie, Y. J. Liu, K. Yan, J. H. Hong, C. H. Jin, Y. Zhou, J. B. Yin, Z. F. Liu and H. L. Peng, *ACS Nano*, 2014, **8**, 1485–1490.
24 S. R. Tamalampudi, Y. Y. Lu, U. R. Kumar, R. Sankar, C. D. Liao, B. K. Moorthy, C. H. Cheng, F. C. Chou and Y. T. Chen, *Nano Lett.*, 2014, **14**, 2800–2806.
25 D. D. Vaughn, R. J. Patel, M. A. Hickner and R. E. Schaak, *J. Am. Chem. Soc.*, 2010, **132**, 15170–15172.
26 C. Li, L. Huang, G. P. Snigdha, Y. F. Yu and L. Y. Cao, *ACS Nano*, 2012, **6**, 8868–8877.
27 J. L. Cao, Z. X. Wang, X. Y. Zhan, Q. S. Wang, M. Safdar, Y. J. Wang and J. He, *Nanotechnology*, 2014, **25**, 105705.
28 L. Li, Z. Chen, Y. Hu, X. W. Wang, T. Zhang, W. Chen and Q. B. Wang, *J. Am. Chem. Soc.*, 2013, **135**, 1213–1216.
29 A. Yamamoto, A. Syouji, T. Goto, E. Kulatov, K. Ohno, Y. Kawazoe, K. Uchida and N. Miura, *Phys. Rev. B: Condens. Matter*, 2001, **64**, 035210.
30 F. C. Liu, H. Shimotani, H. Shang, T. Kanagasekaran, V. Zolyomi, N. Drummond, V. I. Fal'ko and K. Tanigaki, *ACS Nano*, 2014, **8**, 752–760.
31 Y. L. Cui, D. D. Caudel, P. Bhattacharya, A. Burger, K. C. Mandal, D. Johnstone and S. A. Payne, *J. Appl. Phys.*, 2009, **105**, 053709.
32 P. G. Hu, J. Zhang, M. N. Yoon, X. F. Qiao, X. Zhang, W. Feng, P. H. Tan, W. Zheng, J. J. Liu, X. N. Wang, J. C. Idrobo, D. B. Geohegan and K. Xiao, *Nano Res.*, 2014, **7**, 694–703.
33 Z. X. Wang, M. Safdar, C. Jiang and J. He, *Nano Lett.*, 2012, **12**, 4715–4721.
34 S. Najmaei, Z. Liu, W. Zhou, X. L. Zou, G. Shi, S. D. Lei, B. I. Yakobson, J. C. Idrobo, P. M. Ajayan and J. Lou, *Nat. Mater.*, 2013, **12**, 754–759.

35 Y. Zhu, Y. Zhou, M. I. B. Utama, M. de la Mata, Y. Y. Zhao, Q. Zhang, B. Peng, C. Magen, J. Arbiol and Q. H. Xiong, *Nanoscale*, 2013, **5**, 7242–7249.
36 H. Li, J. Cao, W. S. Zheng, Y. L. Chen, D. Wu, W. H. Dang, K. Wang, H. L. Peng and Z. F. Liu, *J. Am. Chem. Soc.*, 2012, **134**, 6132–6135.
37 H. Fang, S. Chuang, T. C. Chang, K. Takei, T. Takahashi and A. Javey, *Nano Lett.*, 2012, **12**, 3788–3792.
38 W. J. Zhang, J. K. Huang, C. H. Chen, Y. H. Chang, Y. J. Cheng and L. J. Li, *Adv. Mater.*, 2013, **25**, 3456–3461.
39 D. K. Kim, Y. M. Lai, T. R. Vemulkar and C. R. Kagan, *ACS Nano*, 2011, **5**, 10074–10083.
40 Q. L. Li, Y. Li, J. Gao, S. D. Wang and X. H. Sun, *Appl. Phys. Lett.*, 2011, **99**, 2436105.
41 R. F. Service, *Science*, 2006, **312**, 1593–1594.
42 A. Marschilok, C. Y. Lee, A. Subramanian, K. J. Takeuchi and E. S. Takeuchi, *Energy Environ. Sci.*, 2011, **4**, 2943–2951.
43 M. C. McAlpine, H. Ahmad, D. W. Wang and J. R. Heath, *Nat. Mater.*, 2007, **6**, 379–384.
44 Z. R. Wang, H. Wang, B. Liu, W. Z. Qiu, J. Zhang, S. H. Ran, H. T. Huang, J. Xu, H. W. Han, D. Chen and G. Z. Shen, *ACS Nano*, 2011, **5**, 8412–8419.
45 Z. Y. Yin, H. Li, H. Li, L. Jiang, Y. M. Shi, Y. H. Sun, G. Lu, Q. Zhang, X. D. Chen and H. Zhang, *ACS Nano*, 2012, **6**, 74–80.
46 H. Kind, H. Q. Yan, B. Messer, M. Law and P. D. Yang, *Adv. Mater.*, 2002, **14**, 158–160.

